12-13-2022

Rapid astrocyte-dependent facilitation amplifies multi-vesicular release in hippocampal synapse

Jongyun Myeong
Washington University School of Medicine in St. Louis
Vitaly A Klyachko
Washington University School of Medicine in St. Louis

Cell Reports

Rapid astrocyte-dependent facilitation amplifies multi-vesicular release in hippocampal synapses

Graphical abstract

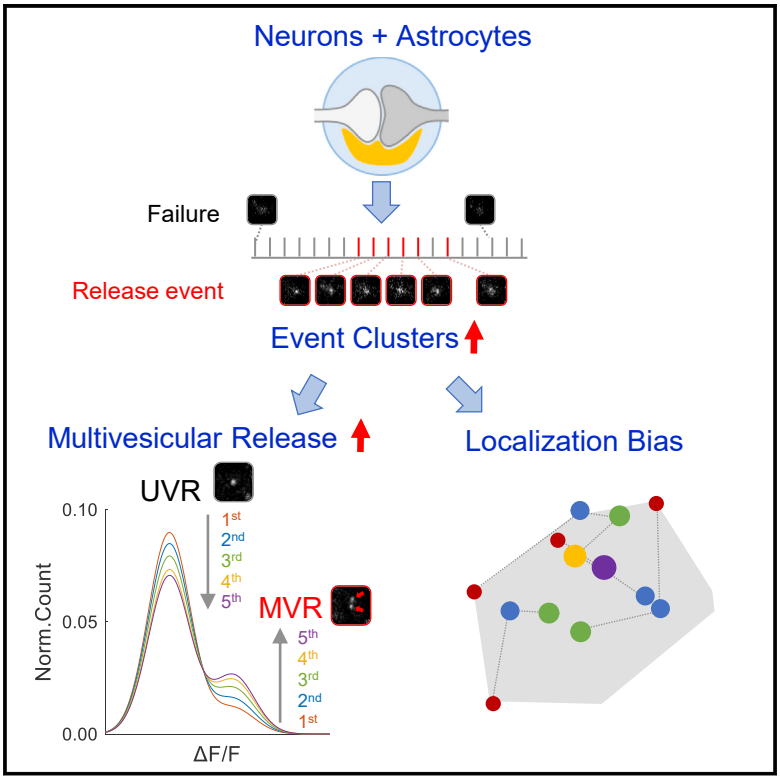

Authors

Jongyun Myeong, Vitaly A. Klyachko

Correspondence

klyachko@wustl.edu

In brief

Myeong and Klyachko report an astrocyte-dependent form of synaptic facilitation triggered by a single glutamate release event and operating at subsecond timescales. Astrocyte-driven facilitation dynamically amplifies multi-vesicular release and induces release events with distinctive spatial organization. The rapid timescale of this modulation suggests that astrocytes may contribute to synaptic computations.

Highlights

- Release events are detected with a near-TIRF approach in hippocampal synapses
- A single release event can trigger astrocyte-dependent facilitation within 500 ms
- Astrocyte-dependent facilitation enhances multi-vesicular release
- Astrocyte-dependent release events have a distinctive spatial organization

Myeong & Klyachko, 2022, Cell Reports *41*, 111820
December 13, 2022
https://doi.org/10.1016/j.celrep.2022.111820

Cell Reports

CellPress
OPEN ACCESS

Report

Rapid astrocyte-dependent facilitation amplifies multi-vesicular release in hippocampal synapses

Jongyun Myeong[1] and Vitaly A. Klyachko[1,2,*]
[1]Department of Cell Biology and Physiology, Washington University School of Medicine, St. Louis, MO 63132, USA
[2]Lead contact
*Correspondence: klyachko@wustl.edu
https://doi.org/10.1016/j.celrep.2022.111820

SUMMARY

Synaptic facilitation is a major form of short-term plasticity typically driven by an increase in residual presynaptic calcium. Using near-total internal reflection fluorescence (near-TIRF) imaging of single vesicle release in cultured hippocampal synapses, we demonstrate a distinctive, release-dependent form of facilitation in which probability of vesicle release is higher following a successful glutamate release event than following a failure. This phenomenon has an onset of $\leq$500 ms and lasts several seconds, resulting in clusters of successful release events. The release-dependent facilitation requires neuronal contact with astrocytes and astrocytic glutamate uptake by EAAT1. It is not observed in neurons grown alone or in the presence of astrocyte-conditioned media. This form of facilitation dynamically amplifies multi-vesicular release. Facilitation-evoked release events exhibit spatial clustering and have a preferential localization toward the active zone center. These results uncover a rapid astrocyte-dependent form of facilitation acting via modulation of multi-vesicular release and displaying distinctive spatiotemporal properties.

INTRODUCTION

Facilitation is a major form of short-term synaptic plasticity enhancing neurotransmitter release on timescales from tens to hundreds of milliseconds.[1,2] Mechanistically, facilitation is widely believed to be a cell-autonomous phenomenon arising from a build up of residual presynaptic calcium during elevated neural activity.[1–3] Facilitation enables synapses to perform a variety of computations[1,3] and is implicated in working memory.[4–7]

Neurotransmitter release is known to be modulated by astrocytes.[8–13] Glutamate released from presynaptic boutons is taken up by astrocytic EAAT1 and EAAT2 transporters, which supply precursors for astrocytic transmitters.[8,14] Presynaptically released glutamate also induces Ca^{2+} release from the astrocytes' intracellular stores via activation of astrocytic mGluR5, subsequently triggering the release of gliotransmitters.[8,11,14–17] Via this bidirectional communication, astrocytes can exert a powerful control of neurotransmission, although direction and timing of this modulation remain debatable. In the hippocampus, there is evidence that astrocytes enhance basal synaptic transmission via the release of ATP (which is converted to adenosine) and the activation of presynaptic adenosine A2 receptors.[11] In contrast, other studies found that astrocytes release glutamate to transiently enhance neurotransmitter release,[12,14,18,19] which is subsequently counteracted by the release of ATP, resulting in synaptic depression.[10,19] Moreover, estimates for the time course of gliotransmission indicate that both potentiating and depressing effects of astrocyte signaling have onset and duration on the order of tens of seconds to several minutes,[11,19] leading some studies to suggest that astrocytes modulate synaptic transmission primarily in a tonic fashion and largely independently of rapid changes in neuronal activity.[11] Yet, a much faster astrocyte signaling mechanism mediated by astrocyte calcium microdomains in close proximity to neurons has also been recently described.[15,16] How this signaling mechanism regulates synaptic transmission is yet to be determined. Thus, whether astrocytes can regulate rapid forms of synaptic dynamics, such as facilitation, remains poorly understood.

Here, we used a near-total internal reflection fluorescence (TIRF) imaging of single-vesicle release in hippocampal synapses to examine how neurotransmitter release is rapidly regulated at the level of individual release events and to define the role of astrocytes in this modulation.

RESULTS

Single glutamate release events can trigger rapid astrocyte-dependent facilitation

To study synaptic dynamics, we performed detection of individual synaptic vesicle release events using a vesicle-bound, pH-sensitive indicator pHluorin (VGlut1-pHluorin)[20–23] expressed in hippocampal synapses in neuron-astrocyte co-cultures (Figure 1A). A near-TIRF approach allowed robust detection of individual release events evoked by 1 Hz stimulation for 200s with improved signal-to-noise ratio and localization precision (Figures S1A and S1B). While detected events had a typical

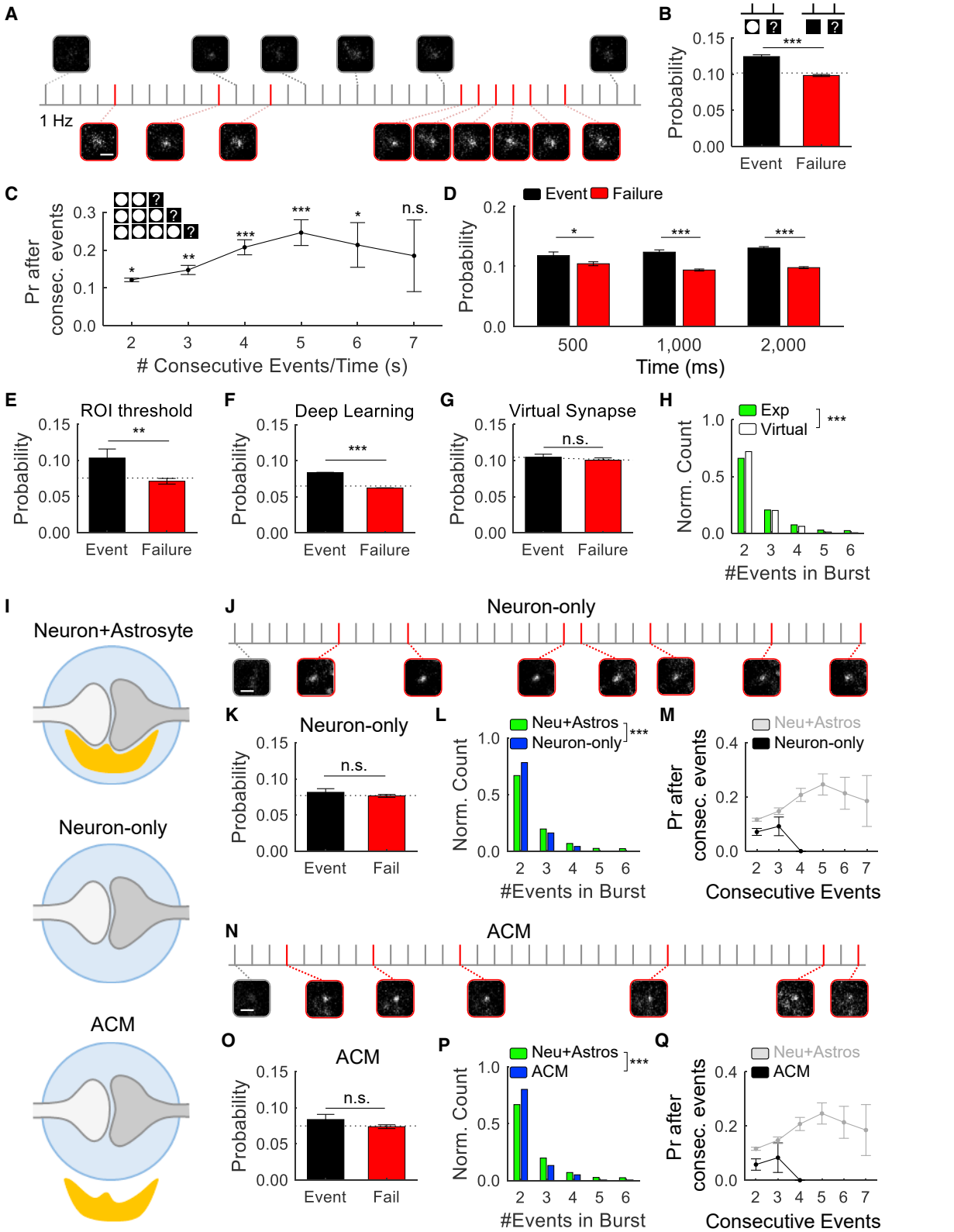

(legend on next page)

average release probability (Pr) of ~0.10, in line with previous studies,[24,25] we noted heterogeneity in their temporal pattern that was evident by the presence of clusters of consecutive events at individual boutons (Figure 1A). To better understand this phenomenon, we compared the Pr for the stimulus immediately following a successful release event (post-event) versus that following a failure (post-failure) at individual boutons. The post-event Pr was significantly higher than the Pr post-failure ($p < 0.001$, two-sample t test, 34,777 events, 308,260 failures, 1,732 boutons from 11 independent cultures) (Figure 1B; Table S1 contains statistical data for all measurements). In other words, at 1 Hz stimulation, the Pr was higher following a release event than following a failure, thus representing a unitary form of synaptic facilitation. This increase in Pr was even larger following several consecutive release events (up to 7 consecutive events were detected) (Figure 1C). The magnitude of the Pr increase scaled with the number of consecutive release events in these clusters or "bursts" up to ~5–6 events (with maximal Pr = 0.246 ± 0.039 after 5 events; Figure 1C), suggesting that this form of facilitation can last several (~5) seconds. To examine the temporal onset of this form of facilitation, we determined the Pr at different time intervals following a stimulus. The smallest interval we could use was 500 ms because the canonical residual-calcium-dependent facilitation, which decays with a ~150 ms time constant at 37°C,[26,27] starts to affect the Pr at shorter intervals, and the two forms of facilitation cannot be distinguished. A small but significant difference in Pr post-event versus post-failure could already be detected 500 ms following a release event (Figure 1D). In line with the observations above (Figure 1C), the Pr increase was more robust 2,000 ms following a release event (Figure 1D), together suggesting that this form of facilitation is detectable as early as 500 ms and lasts several seconds. Here, we refer to this phenomenon as release-dependent facilitation.

To exclude a possibility that our detection algorithm influenced these observations, we confirmed these results with three independent approaches. First, we applied an entirely different algorithm for event detection using thresholds on fluorescence intensity and its slope in the synapse region of interest (ROI) (Figure S1C),[28] which confirmed a significantly higher Pr post-event versus post-failure (Figure 1E). Second, we employed a deep-learning algorithm for event detection (Figures S1D and S1E) and obtained essentially the same result (Figure 1F). Finally, a basic virtual synapse model with the same number of release events as observed in experiments, but evoked randomly in time (Figure S1F), did not exhibit differences in Pr post-event versus post-failure (Figure 1G) and had a significantly smaller number of consecutive release events than observed in experiments (Figure 1H). Together, these results strongly support the above observations of a release-dependent facilitation.

In contrast with the canonical facilitation, release-dependent facilitation cannot arise simply from an increase in residual presynaptic calcium because every action potential (AP) evokes similar calcium rise,[29,30] yet facilitation was observed only following successful release events but not failures. Astrocytes are known to sense glutamate released from presynaptic terminals and to regulate synaptic transmission,[8] although the astrocyte-dependent modulation reported thus far was found to operate on much slower timescales.[11,19] We thus asked if the release-dependent facilitation was astrocyte dependent by comparing properties of vesicle release in three conditions: (1) neurons grown in direct contact with astrocytes on the astrocyte feeder layer as in experiments above, (2) pure neuronal cultures grown without astrocytes, and (3) neurons grown in astrocyte-conditioned medium (ACM) but without direct contact with astrocytes (Figure 1I). We found that release events in neuron-only or ACM conditions did not show any differences in Pr following successful events versus failures (Figures 1J, 1K, 1N, and 1O), and no significant increase in Pr was observed even following multiple consecutive release events (Figures 1M and 1Q). Moreover, the number of consecutive release events detected in both conditions was significantly reduced compared with neurons grown in direct contact with astrocytes (Figures 1L, 1M, 1P, and 1Q). These observations suggest that release-dependent facilitation requires dynamic neuron-astrocyte interaction.

To confirm these observations using an independent approach, we performed imaging of glutamate release at single synapses using glutamate sensor SF-iGluSnFR(A184S)[31] expressed selectively in neurons (Figure S2A). Under the same experimental conditions, this imaging tool provided a robust detection of individual glutamate release events with the same basal Pr as was observed using VGlut1-pHluorin

Figure 1. Single vesicle release events trigger rapid astrocyte-dependent facilitation

(A) Sample temporal distribution and representative images of single release events (red bars) or failures (gray bars) evoked by 1 Hz stimulation in a single bouton in a neuron-astrocyte co-culture. Scale bar is 1 μm.

(B) Pr measured 1 s post-event or 1 s post-failure, calculated for each stimulus at 1 Hz for 200 s. Dashed line represents average basal Pr.

(C) Pr measured 1 s following "bursts" of several (2–7) consecutive release events, representing a conditional Pr of observing another consecutive release event if a burst of given size is observed. At the 1 Hz stimulation used, the number of consecutive events is the same as the timescale in seconds.

(D) Pr post-event and post-failure assessed at 500, 1,000, or 2,000 ms stimulation intervals.

(E) Same as (B) determined by ROI threshold/slope analysis.

(F) Same as (B) determined by the deep-learning algorithm.

(G) Same as (B) for virtual model synapses with the same number of events but distributed randomly in time.

(H) The number of consecutive events detected in each burst compared with virtual synapses.

(I) Schematic of 3 different neuronal culture conditions used.

(J and K) Same as (A) and (B) for neurons grown alone.

(L) Number of consecutive events per "burst" for neurons grown alone versus neurons grown with astrocytes.

(M) Same as (C) for neurons grown alone versus neurons grown with astrocytes.

(N–Q) Same as (J)–(M) for neurons grown in ACM.

Data are reported as mean ± SEM. 9–38 coverslips from 3 to 11 independent cultures (Table S1). *$p < 0.05$, **$p < 0.01$, ***$p < 0.001$, n.s., not significant. Two-sample t test or K-S test (Table S1).

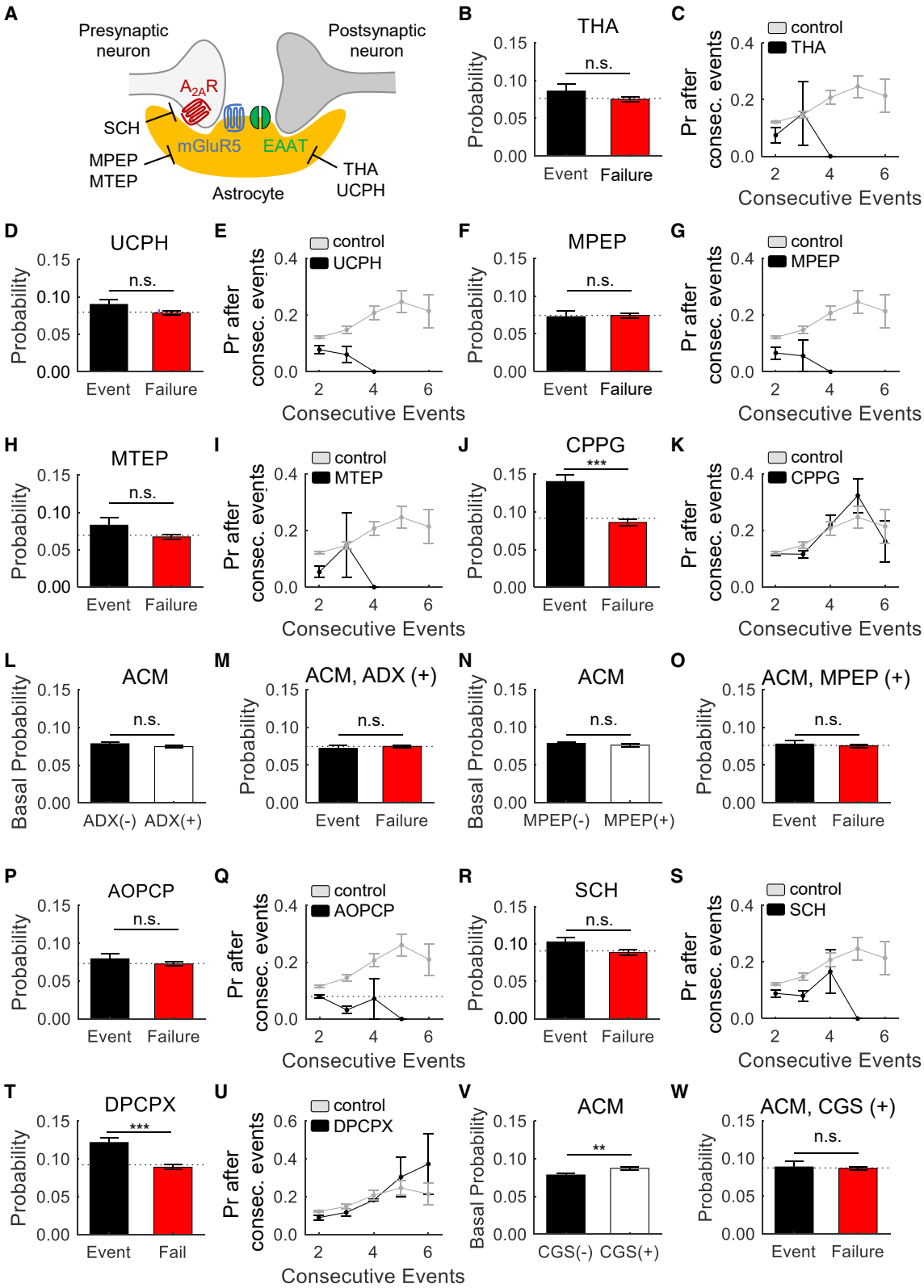

(legend on next page)

(iGluSnFR: 0.091 ± 0.007; VGlut1-pHluorin: 0.101 ± 0.002; p = 0.21, Kolmogorov-Smirnov [K-S] test). Most importantly, in neurons grown in direct contact with astrocytes, the post-event Pr was significantly higher than the Pr post-failure (Figures S2A and S2B), while no difference in Pr was observed in ACM conditions (Figures S2C and S2D). We verified that astrocytes in culture conditions can robustly sense synaptically released glutamate using a selective expression of iGluSnFR in astrocytes (GFAP.SF-iGluSnFR(A184S)[31]; Figures S2E–S2J). These observations provide an independent confirmation for the release-dependent facilitation that requires direct neuron-astrocyte interaction.

Release-dependent facilitation requires bidirectional neuron-astrocyte signaling

To support the role of astrocytes in release-dependent facilitation, we next examined the transporters/receptors that are required in this phenomenon (Figure 2A).

Glutamate converted to gliotransmitters is taken up through astrocytic transporters EAAT1 and EAAT2.[14] We tested their involvement in release-dependent facilitation using 30 min preincubation with a potent EAAT1/EAAT2 inhibitor, THA. THA eliminated differences in Pr post-event versus post-failure (Figure 2B). Moreover, THA blocked the increase in Pr following multiple consecutive events (Figure 2C) and markedly reduced the number of consecutive release events detected (Figures 2C and S3A), thus effectively abolishing the release-dependent facilitation. Furthermore, preincubation with a selective EAAT1 inhibitor UCPH-102 was sufficient to abolish all of these measures of release-dependent facilitation (Figures 2D, 2E, and S3B), supporting the notion that this form of facilitation is astrocyte-dependent and requires EAAT1.

We next probe the involvement of the well-established astrocyte signaling cascade of gliotransmitter release involving activation of astrocytic mGluR5[32,33] and subsequently presynaptic adenosine receptors[11] in release-dependent facilitation. Preincubation with selective mGluR5 antagonists MPEP or MTEP abolished all measures of release-dependent facilitation (Figures 2F–2I, S3C, and S3D). In contrast, CPPG, a selective antagonist of group II/III mGluRs, had no effect (Figures 2J, 2K, and S3E). Importantly, in the absence of neuron-astrocyte contact (i.e., in ACM conditions), neither enhancement of mGluR5 activity with a positive allosteric modulator ADX-47273 nor inhibition of mGluR5 with MPEP had any measurable effect on the basal Pr (Figures 2L and 2N) nor on the Pr post-event or Pr post-failure (Figures 2M and 2O). This excludes the presynaptic contribution of mGluR5 to Pr modulation in general and to release-dependent facilitation specifically. Thus, mGluR5 must act in astrocytes to mediate release-dependent facilitation. This is also consistent with the previous immunohistochemical analyses of astrocyte-synapse contacts, showing predominant mGluR5 localization in astrocytes and neuronal dendrites but not in presynaptic boutons.[11,34–36]

ATP released from astrocytes is degraded to adenosine, which modulates synaptic transmission via activation of presynaptic adenosine receptors.[10,11,37] Accordingly, we observed that AOPCP, a selective inhibitor of ecto-5′-nucleotidase (CD73) that hydrolyzes AMP to adenosine, abolished release-dependent facilitation (Figures 2P and 2Q), thus supporting the importance of adenosine in this phenomenon. We next tested the role of adenosine receptors and found that a selective A_{2A} receptor antagonist, SCH-58261, strongly reduced release-dependent facilitation (Figures 2R, 2S, and S3F), while the A_{1A} receptor antagonist DPCPX had no effect (Figures 2T, 2U, and S3G). Moreover, direct activation of A_{2A} receptors with agonist CGS21680 in the absence of neuron-astrocyte contact (i.e., in ACM) significantly increased the average Pr during 1 Hz stimulation (Figure 2V), thus mimicking the effect of astrocytes during release-dependent facilitation. However, direct A_{2A} activation by an agonist effectively "facilitates" all release events equally and thus is not expected to produce differences in Pr between post-event and post-failure, which is indeed what we observed in ACM conditions (Figure 2W). Together, these results support the role of presynaptic A_{2A} receptors in release-dependent facilitation.

We note that inhibition of release-dependent facilitation by various treatments cannot be explained by resetting of basal Pr. Facilitation is typically inversely correlated with Pr such that synapses with higher basal Pr exhibit smaller facilitation.[38] In contrast, basal Pr was unchanged or slightly reduced in all conditions in which release-dependent facilitation was blocked (Figure 2).

Figure 2. Signaling pathway mediating astrocyte-dependent facilitation

(A) Partial schematic of the synapse/astrocyte contact with relevant receptors, transporters, and their blockers.

(B) Pr post-event and post-failure after 30 min preincubation with 100 μM THA in neuron-astrocyte co-culture. Dashed line represents average basal Pr.

(C) Pr measured 1 s following "bursts" of different duration in untreated neuron-astrocyte co-cultures (pooled control, gray) or after 30 min preincubation with 100 μM THA (black).

(D and E) Same as (B) and (C) for 10 μM UCPH-102.

(F and G) Same as (B) and (C) for 250 μM MPEP.

(H and I) Same as (B) and (C) for 250 μM MTEP.

(J and K) Same as (B) and (C) for 100 nM CPPG.

(L) Average basal Pr in ACM conditions with (white) or without (black) 30 min preincubation with 1 μM ADX47273.

(M) Same measurements as (B) for 1 μM ADX47273 in ACM conditions.

(N and O) Same as (L) and (M) for 250 μM MPEP in ACM conditions.

(P and Q) Same as (B) and (C) for 100 μM AOPCP.

(R and S) Same as (B) and (C) for 100 nM SCH58261.

(T and U) Same as (B) and (C) for 1 μM DPCPX.

(V and W) Same as (L) and (M) for 100 nM CGS21680 in ACM conditions.

Data are reported as mean ± SEM. 6–17 coverslips from 3 to 6 independent cultures (Table S1). $^{**}p < 0.01$, $^{***}p < 0.001$, n.s., not significant. Two-sample t test (see Table S1).

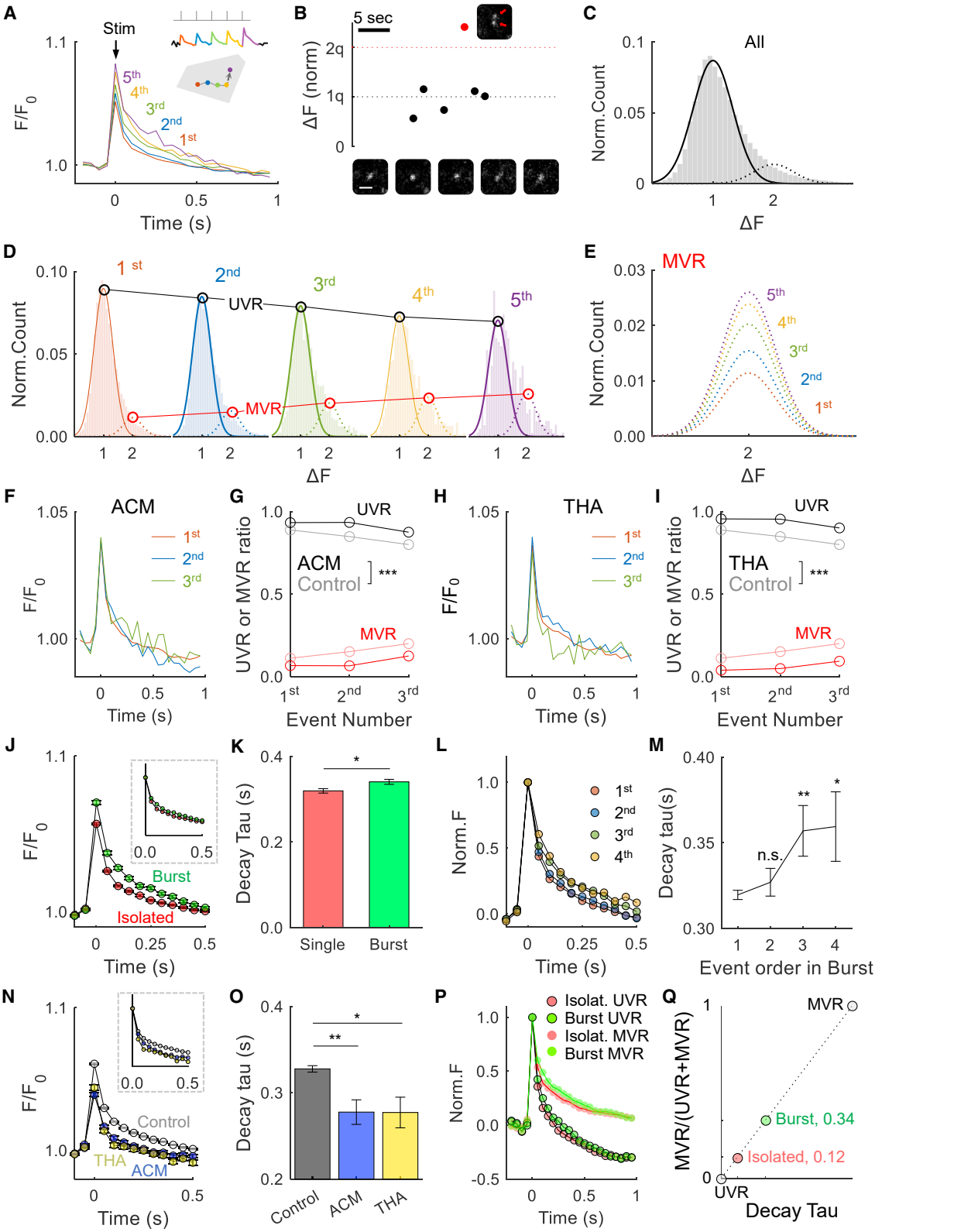

(legend on next page)

These results support our findings above that release-dependent facilitation is an astrocyte-dependent phenomenon since it requires astrocytic EAAT1 transporters and utilizes a well-established astrocyte-neuron signaling pathway involving mGluR5-dependent astrocytic ATP release.[11,32,33]

Astrocyte-dependent facilitation potentiates multi-vesicular release

We made an unexpected observation that consecutive release events during release-dependent facilitation had a larger average amplitude than isolated events, and this amplitude increase became more prominent with the burst progression in time (Figure 3A). Since the average release event amplitude is strongly affected by the prevalence of univesicular release (UVR) versus multi-vesicular release (MVR),[39,40] we hypothesized that this phenomenon could arise from an increased proportion of MVR events during release-dependent facilitation. MVR is ubiquitously observed in central synapses[39]; in our measurements, MVR is most commonly observed as a near-simultaneous release of two vesicles[40] (Figure 3B). Such events are evident in the amplitude distribution of individual events by their double quantal amplitude (Figures 3B and 3C). Whether astrocytes can regulate prevalence of MVR remains unknown.

To examine this hypothesis quantitatively, we applied an established bi-Gaussian fitting approach of the event amplitude distribution to determine the proportion of UVR to MVR events (Figure 3C).[40] We found a progressive increase in the proportion of MVR during bursts, reaching 2- to 3-fold toward the end of the bursts (Figures 3D, 3E, S4A, and S4B). Importantly, this increase in MVR was greatly diminished in neurons grown in ACM (Figures 3F and 3G) or in the presence of EAAT inhibitor THA (Figures 3H and 3I), indicating that it was astrocyte dependent.

In parallel with the increased proportion of MVR during bursts, the average decay kinetics of release events became progressively slower (Figures 3J–3M). These changes in event kinetics were also astrocyte dependent (Figures 3N and 3O). To determine if these two observations represent the same or two distinct phenomena, we performed detection of all UVR and MVR events in each synapse[40] and found that MVR events have a significantly slower decay kinetics than UVR events (Figures S4C and S4D). Yet, the identified UVR events showed no differences in kinetics between isolated and burst events, and the same was the case for the MVR events (Figures 3P and S4E). Thus, the slower average event decay kinetics during bursts was not due to changes in the properties of individual release events. To further support this point, we asked if the proportion of UVR to MVR can be predicted solely based on the differences in their decay kinetics. Assuming the simplest, linear relationship between the two parameters, we obtained estimates of 12% of MVR for isolated events and 34% of MVR for burst events (Figure 3Q). This is in good agreement with ~10% of MVR among isolated events as determined by the event detection (Figure 3B, and see the first peak in Figure 3D) and the observed 2- to 3-fold increase in MVR during bursts (Figures 3D and 3E). Thus, a larger proportion of MVR events during bursts fully accounts for the slower event decay kinetics. We note that in contrast to the MVR events, isolated asynchronous events have a faster decay kinetics than UVR events (UVR: 0.32 ± 0.003 s; asynchronous events: 0.27 ± 0.003 s, $p < 0.001$, t test). Thus, the increase in asynchronous events cannot account for the slower event decay kinetics during bursts. Taken together, these results indicate that astrocytes rapidly and dynamically modulate prevalence of MVR during release-dependent facilitation.

Why do some release events trigger astrocyte-dependent facilitation and some do not? Since this phenomenon is initiated by glutamate release, we asked if MVR events, which presumably release more glutamate than UVR events, are also more likely to initiate release-dependent facilitation. We found that Pr was indeed significantly higher post-MVR than post-UVR events (Figure S4F), and the probability of observing bursts with three or more consecutive events was also significantly higher following MVR events (Figure S4G). However, having MVR was not a necessary condition since bursts were also frequently evoked by UVR events. Thus, additional factors, such as possibly the proximity of the release events to the astrocyte processes and/or other factors, work together with the mode of vesicle release to determine which release events are capable of triggering astrocyte-dependent facilitation.

Figure 3. Astrocyte-dependent facilitation potentiates multi-vesicular release

(A) Average traces of consecutive release events (from first to fifth) during bursts (schematic above), each recorded for 1 s following an AP (Stim).

(B) 35 s of a sample recording with identified UVR (black) and MVR (red) release events in a single bouton with corresponding images. Scale bar is 1 μm.

(C) Amplitude histogram of all detected events with two peaks corresponding to UVR (1q) and MVR (2q) events and their corresponding Gaussian fits.

(D) Same as (C) shown separately for each of consecutive events during bursts from first to fifth.

(E) Gaussian fits of the MVR peaks from (D) for consecutive events in the bursts from first to fifth.

(F) Average traces of consecutive release events during bursts in neurons grown in ACM.

(G) Relative proportion of UVR (black) and MVR (red) events during bursts in ACM conditions (dark lines) compared with control (untreated astrocyte-neuronal co-culture, light lines).

(H and I) Same as (F) and (G) for neurons pretreated with 100 μM THA.

(J and K) Average fluorescence traces of all isolated events versus all burst events (J) and corresponding kinetics of decay (K). Inset in (J), individual event traces were normalized to peak, averaged and plotted from T = 0.

(L and M) Average normalized traces (L) and their decay kinetics (M) for consecutive events during bursts separated by their order in the bursts from first to fourth.

(N and O) Average fluorescence traces of all detected events (N) and their decay kinetics (O) for control (untreated astrocyte-neuronal co-culture) compared with neurons grown in ACM or pretreated with THA. Inset in (N), individual event traces were normalized to peak, averaged and plotted from T = 0.

(P) Average normalized traces of isolated UVR and MVR events and of UVR and MVR events during bursts.

(Q) UVR/MVR ratio for isolated events or burst events predicted from the average event decay kinetics.

Data are reported as mean ± SEM. 15–38 coverslips from 4 to 11 independent cultures (Table S1). *$p < 0.05$, **$p < 0.01$, ***$p < 0.001$, n.s., not significant. Two-sample t test, K-S test, or ANOVA (see Table S1).

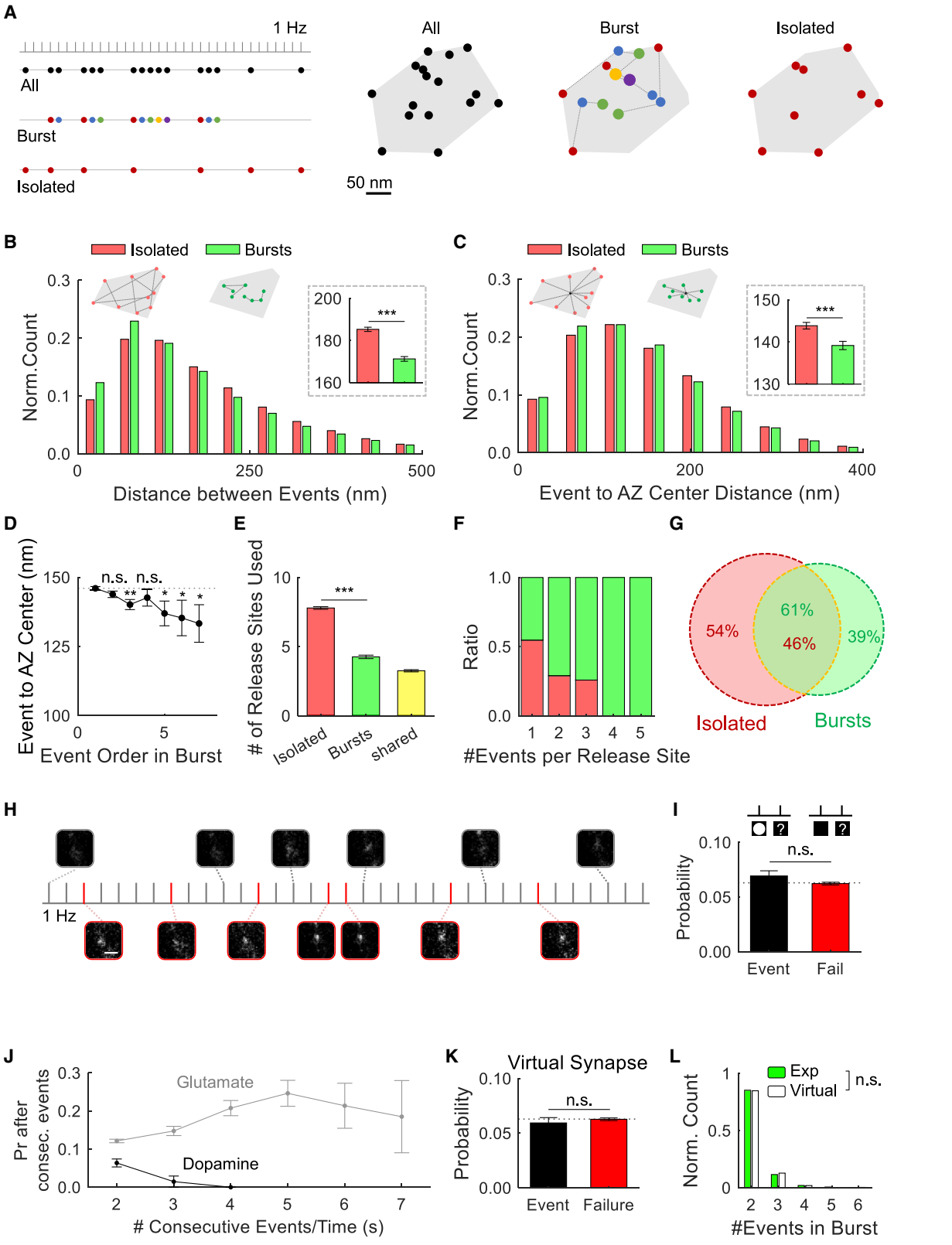

(legend on next page)

Distinctive spatiotemporal properties of astrocyte-dependent release events

Various forms of vesicle release, including UVR, MVR, and asynchronous release, have different spatial distributions across the active zone (AZ).[23,40–42] We thus asked if spatial organization of astrocyte-dependent release events is distinct from other release events.

First, we observed that the consecutive events during bursts occurred at significantly shorter distances from each other than isolated events (Figures 4A and 4B), suggesting that burst events exhibit spatial clustering. Moreover, burst events were localized significantly closer to the AZ center than isolated events (Figure 4C), and this spatial bias toward the AZ center increased progressively as bursts evolved in time (Figure 4D). Release events evoked by astrocyte-dependent facilitation thus have distinctive spatial properties characterized by spatial clustering and a bias toward the AZ center.

Vesicle release occurs at several (~4–15) release sites undergoing repeated reuse.[23,43] We thus next ask if a subset of release sites is preferentially utilized during astrocyte-dependent facilitation. Release sites within each bouton were defined using a hierarchical clustering algorithm[23,40] using isolated events only. In this analysis, we examined synapses with a minimum of 15 detected events because a smaller number of events may not fully sample all existing release sites during the limited observation period. Events during bursts utilized a significantly smaller number of release sites (Figure 4E) and were ~3-fold more likely to occur at the same release site than isolated events (Figure 4F). Burst events also preferentially utilized release sites localized closer to the AZ center (Figure S4H), in line with the findings above. This differential utilization of release sites is also reflected in only a partial overlap/co-occurrence of isolated and burst events at the same release sites during the observation period (Figure 4G). This was not due to selection of a subset of most active synapses since nearly the same degree of overlap was also observed in a much larger synapse population with 10 or more release events detected (Figures S4I and S4J).

Taken together, these results suggest that events evoked during astrocyte-dependent facilitation preferentially cluster at a subset of available release sites with a bias toward the AZ center.

Astrocyte-dependent facilitation is specific to glutamate release and does not regulate dopamine release in hippocampal synapses

Recent studies found that in addition to glutamate, a subset of excitatory hippocampal synapses releases dopamine.[44] Thus, we asked whether astrocyte-dependent facilitation is specific to glutamate release or also regulates release of other neurotransmitters, such as dopamine. To address this question, we visualized dopamine release by expressing a vMAT2-pHluorin in hippocampal synapses, as described.[44] Single-vesicle dopamine release events were reliably detected in hippocampal synapses (Figure 4H) with localization precision (15.4 ± 0.1 nm) and peak SNR (PSNR; 119.1 ± 1.6) comparable to that of glutamate release events. Dopamine release had a lower average Pr of ~0.06, which is in line with the previous study.[44] Most importantly, in contrast with glutamate release, dopamine release events showed no differences in Pr following successful events versus failures (Figure 4I). Moreover, there was no increase in Pr observed following multiple consecutive dopamine release events, and the number of consecutive events detected was greatly reduced compared with glutamate release events (Figure 4J). In fact, dopamine release was indistinguishable in its temporal properties from a virtual synapse with release events occurring randomly in time (Figures 4K and 4L). These results indicate that at least for the hippocampal synapses in culture, astrocyte-dependent facilitation is specific to glutamate release.

DISCUSSION

One of the dogmas in synaptic physiology postulated that vesicle release events evoked by single APs are random and independent from each other in the absence of high-frequency activity.[45,46] An increase in Pr can then occur in response to rapid neuronal firing due to accumulation of residual presynaptic calcium, which causes facilitation of release.[47,48] Our results uncover a distinctive, astrocyte-dependent form of synaptic facilitation operating at a subsecond timescale and capable of modifying synaptic strength in response to a single release event. These results also indicate that glutamate release events are not entirely independent in the presence of astrocytes but

Figure 4. Distinctive spatiotemporal organization and specificity of astrocyte-dependent facilitation

(A) Sample AZ with localization of release events detected during 35 s of a sample recording (right panels). Isolated events (red) and burst events (colors) are shown separately for the same AZ. Burst progression over time is shown with increasing dot size and color sequence (same as in Figures 3A and 3D).

(B) Distribution of distances between consecutive events (green) during bursts or between sequential isolated events over time (red). Inset, average distances from the distributions below.

(C) Distribution of distances from release events to the AZ center for events during bursts (green) or isolated events (red). Inset, average distances from the distributions below.

(D) Average distance to AZ center calculated separately for each of the consecutive events during bursts.

(E) Average number of release sites per bouton utilized by isolated events (red), events during bursts (green), or both (yellow, shared release sites).

(F) Proportion of isolated events (red) to burst events (green) at release sites with various number of detected events.

(G) Venn diagram showing percentages of isolated events (red) and burst events (green) utilizing the same/distinct release sites.

(H) 35 s of sample temporal distribution and representative images of vMAT2-pHluorin events evoked by 1 Hz stimulation in a single hippocampal bouton. Scale bar is 1 μm.

(I) Pr measured 1 s post-event or post-failure for vMAT2-pHluorin events.

(J) Pr measured 1s following "bursts" of consecutive glutamate (gray) or dopamine (black) events of various duration.

(K) Pr post-event versus post-failure for virtual synapses with dopamine release events distributed randomly in time.

(L) The number of consecutive dopamine release events compared with virtual synapses.

Data are reported as mean ± SEM. 22–38 coverslips from 4 to 11 independent cultures (Table S1). *p < 0.05, **p < 0.01, ***p < 0.001, n.s., not significant. Two-sample t test (see Table S1).

can dynamically regulate the temporal and spatial properties of subsequent events via the engagement of astrocyte-dependent facilitation.

Events evoked during astrocyte-dependent facilitation have several distinctive properties, which distinguish this phenomenon from canonical synaptic facilitation. This includes a bias in event localization toward the AZ center and their spatial clustering evident in repetitive utilization of a subset of release sites. Most notably, the two forms of facilitation have different requirements for presynaptic calcium elevation, which was insufficient to trigger release-dependent facilitation. It was only observed after successful release events, but not failures, despite the same AP stimulation and thus presynaptic calcium elevation.[29,30] Instead, this form of facilitation requires glutamate release and a direct neuronal contact with astrocytes. Notably, there is an apparent discrepancy between the rapid subsecond kinetics of this facilitation mechanism and the previously reported timescale of tens of seconds to several minutes observed for the glutamate-evoked calcium elevation in astrocytes and subsequent feedback signaling to neurons.[11,12,19] However, this slower timescale of astrocyte-dependent modulation was based on calcium uncaging experiments or observations of global calcium elevation in astrocytes. Instead, a much faster astrocyte response may be mediated by locally restricted calcium microdomains in astrocyte processes and endfeet, which was found to rapidly follow neuronal activation within ~120 ms.[15,16] Our observations are consistent with this rapid local signaling mechanism and suggest that astrocytes not only sense but also rapidly respond to single vesicle release events and can shape synaptic dynamics on a subsecond timescale.

Our results show that astrocyte-dependent facilitation causes a rapid increase in MVR, thus demonstrating that astrocytes can dynamically regulate the synaptic MVR/UVR balance. MVR is a ubiquitous form of neurotransmitter release controlling many critical synaptic functions, including reliability and gain.[39] The prevalence of MVR at individual synapses is not static,[21,49,50] although the mechanisms that regulate the occurrence of MVR remain debatable. MVR is modulated by extracellular calcium levels,[21,49] presynaptic calcium elevation due to changes in Pr,[50] or by cAMP/PKA-dependent modulation of the readily releasable pool size in the absence of Pr changes.[51] Interestingly, during astrocyte-induced facilitation, the MVR/UVR ratio increases nearly linearly with the number of release events, at least at the 1 Hz stimulation frequency used. Given the established roles for MVR in controlling synaptic gain,[39] it will be interesting to determine in future studies if this near-linear scaling of MVR may serve computational purposes. Indeed, facilitation plays many important roles in synaptic computations[1,3,27,52,53] and, together with its longer form, known as augmentation, may also function as cellular substrate for working memory.[4–7] Recently, a model of working memory incorporating interacting networks of neurons and astrocytes with cross-modulation on a timescale of ~10 s could successfully store memories of recent neuronal activity.[54] The astrocyte-dependent facilitation described here operates on timescales between the canonical facilitation (~150 ms) and augmentation (~5–10s). While defining specific functions for the astrocyte-dependent facilitation will require extensive future investigation, its properties and timescale suggest an intriguing possibility that astrocytes may modulate many fundamental information processing operations, including working memory.

Limitations of the study

The important unresolved question in our study is why some release events are able to trigger astrocyte-dependent facilitation while others are not. Moreover, understanding how this form of facilitation is rapidly terminated will require further investigation. In addition, astrocyte-neuron interactions observed in culture conditions may not fully reflect the complex spatial organization and signaling of tripartite synapses *in vivo*. Finally, because of the intrinsic temporal limitations in our recordings caused by the natural displacement of synapses in culture, we cannot fully explore the mechanisms determining the distinct spatial organization of vesicle release driven by astrocyte-dependent facilitation.

STAR★METHODS

Detailed methods are provided in the online version of this paper and include the following:

- KEY RESOURCES TABLE
- RESOURCE AVAILABILITY
  - Lead contact
  - Materials availability
  - Data and code availability
- EXPERIMENTAL MODEL AND SUBJECT DETAILS
- METHOD DETAILS
  - Lentiviral infection
  - Near-TIRF microscopy
  - Experimental design
  - Pharmacology
- QUANTIFICATION AND STATISTICAL ANALYSES
  - Event detection and localization using mixture-model fitting
  - Event detection using deep learning algorithm
  - Event detection using ROI thresholding
  - Virtual model synapse
  - Identification and analysis of MVR events
  - Analysis of event spatial organization
  - Analysis of glutamate transients in astrocytes
  - Data inclusion and exclusion criteria
  - Statistical analysis

SUPPLEMENTAL INFORMATION

Supplemental information can be found online at https://doi.org/10.1016/j.celrep.2022.111820.

ACKNOWLEDGMENTS

This work was supported in part by NIH grant R35 NS111596 to V.A.K.

AUTHOR CONTRIBUTIONS

J.M. and V.A.K. conceived and designed the experiments. J.M. performed all experiments and analyzed the data. Both authors wrote the manuscript and approved the final version.

DECLARATION OF INTERESTS

The authors declare no competing interests.

Received: May 9, 2022
Revised: September 30, 2022
Accepted: November 21, 2022
Published: December 13, 2022

REFERENCES

1. Abbott, L.F., and Regehr, W.G. (2004). Synaptic computation. Nature *431*, 796–803.
2. Jackman, S.L., and Regehr, W.G. (2017). The mechanisms and functions of synaptic facilitation. Neuron *94*, 447–464. https://doi.org/10.1016/j.neuron.2017.02.047.
3. Deng, P.Y., and Klyachko, V.A. (2011). The diverse functions of short-term plasticity components in synaptic computations. Commun. Integr. Biol. *4*, 543–548. https://doi.org/10.4161/cib.4.5.15870.
4. Barak, O., Tsodyks, M., and Romo, R. (2010). Neuronal population coding of parametric working memory. J. Neurosci. *30*, 9424–9430. https://doi.org/10.1523/JNEUROSCI.1875-10.2010.
5. Mongillo, G., Barak, O., and Tsodyks, M. (2008). Synaptic theory of working memory. Science *319*, 1543–1546. https://doi.org/10.1126/science.1150769.
6. Deco, G., Rolls, E.T., and Romo, R. (2010). Synaptic dynamics and decision making. Proc. Natl. Acad. Sci. USA *107*, 7545–7549. https://doi.org/10.1073/pnas.1002333107.
7. Fiebig, F., and Lansner, A. (2017). A spiking working memory model based on hebbian short-term potentiation. J. Neurosci. *37*, 83–96. https://doi.org/10.1523/JNEUROSCI.1989-16.2016.
8. Sancho, L., Contreras, M., and Allen, N.J. (2021). Glia as sculptors of synaptic plasticity. Neurosci. Res. *167*, 17–29. https://doi.org/10.1016/j.neures.2020.11.005.
9. Araque, A., Parpura, V., Sanzgiri, R.P., and Haydon, P.G. (1999). Tripartite synapses: glia, the unacknowledged partner. Trends Neurosci. *22*, 208–215. https://doi.org/10.1016/s0166-2236(98)01349-6.
10. Pascual, O., Casper, K.B., Kubera, C., Zhang, J., Revilla-Sanchez, R., Sul, J.Y., Takano, H., Moss, S.J., McCarthy, K., and Haydon, P.G. (2005). Astrocytic purinergic signaling coordinates synaptic networks. Science *310*, 113–116. https://doi.org/10.1126/science.1116916.
11. Panatier, A., Vallée, J., Haber, M., Murai, K.K., Lacaille, J.C., and Robitaille, R. (2011). Astrocytes are endogenous regulators of basal transmission at central synapses. Cell *146*, 785–798. https://doi.org/10.1016/j.cell.2011.07.022.
12. Perea, G., and Araque, A. (2007). Astrocytes potentiate transmitter release at single hippocampal synapses. Science *317*, 1083–1086. https://doi.org/10.1126/science.1144640.
13. Di Castro, M.A., Chuquet, J., Liaudet, N., Bhaukaurally, K., Santello, M., Bouvier, D., Tiret, P., and Volterra, A. (2011). Local Ca^{2+} detection and modulation of synaptic release by astrocytes. Nat. Neurosci. *14*, 1276–1284. https://doi.org/10.1038/nn.2929.
14. Mahmoud, S., Gharagozloo, M., Simard, C., and Gris, D. (2019). Astrocytes maintain glutamate homeostasis in the CNS by controlling the balance between glutamate uptake and release. Cells *8*. https://doi.org/10.3390/cells8020184.
15. Stobart, J.L., Ferrari, K.D., Barrett, M.J.P., Glück, C., Stobart, M.J., Zuend, M., and Weber, B. (2018). Cortical circuit activity evokes rapid astrocyte calcium signals on a similar timescale to neurons. Neuron *98*, 726–735.e4. https://doi.org/10.1016/j.neuron.2018.03.050.
16. Bindocci, E., Savtchouk, I., Liaudet, N., Becker, D., Carriero, G., and Volterra, A. (2017). Three-dimensional Ca^{2+} imaging advances understanding of astrocyte biology. Science *356*, eaai8185. https://doi.org/10.1126/science.aai8185.
17. Lia, A., Henriques, V.J., Zonta, M., Chiavegato, A., Carmignoto, G., Gómez-Gonzalo, M., and Losi, G. (2021). Calcium signals in astrocyte microdomains, a decade of great advances. Front. Cell. Neurosci. *15*, 673433. https://doi.org/10.3389/fncel.2021.673433.
18. Navarrete, M., and Araque, A. (2010). Endocannabinoids potentiate synaptic transmission through stimulation of astrocytes. Neuron *68*, 113–126. https://doi.org/10.1016/j.neuron.2010.08.043.
19. Covelo, A., and Araque, A. (2018). Neuronal activity determines distinct gliotransmitter release from a single astrocyte. Elife *7*, e32237. https://doi.org/10.7554/eLife.32237.
20. Voglmaier, S.M., Kam, K., Yang, H., Fortin, D.L., Hua, Z., Nicoll, R.A., and Edwards, R.H. (2006). Distinct endocytic pathways control the rate and extent of synaptic vesicle protein recycling. Neuron *51*, 71–84. https://doi.org/10.1016/j.neuron.2006.05.027.
21. Leitz, J., and Kavalali, E.T. (2011). Ca^{2+}influx slows single synaptic vesicle endocytosis. J. Neurosci. *31*, 16318–16326. https://doi.org/10.1523/JNEUROSCI.3358-11.2011.
22. Maschi, D., Gramlich, M.W., and Klyachko, V.A. (2018). Myosin V functions as a vesicle tether at the plasma membrane to control neurotransmitter release in central synapses. Elife *7*, e39440. https://doi.org/10.7554/eLife.39440.
23. Maschi, D., and Klyachko, V.A. (2017). Spatiotemporal regulation of synaptic vesicle fusion sites in central synapses. Neuron *94*, 65–73.e3. https://doi.org/10.1016/j.neuron.2017.03.006.
24. Branco, T., and Staras, K. (2009). The probability of neurotransmitter release: variability and feedback control at single synapses. Nat. Rev. Neurosci. *10*, 373–383. https://doi.org/10.1038/nrn2634.
25. Hessler, N.A., Shirke, A.M., and Malinow, R. (1993). The probability of transmitter release at a mammalian central synapse. Nature *366*, 569–572. https://doi.org/10.1038/366569a0.
26. Klyachko, V.A., and Stevens, C.F. (2006). Temperature-dependent shift of balance among the components of short-term plasticity in hippocampal synapses. J. Neurosci. *26*, 6945–6957.
27. Kandaswamy, U., Deng, P.Y., Stevens, C.F., and Klyachko, V.A. (2010). The role of presynaptic dynamics in processing of natural spike trains in hippocampal synapses. J. Neurosci. *30*, 15904–15914. https://doi.org/10.1523/JNEUROSCI.4050-10.2010.
28. Reese, A.L., and Kavalali, E.T. (2015). Spontaneous neurotransmission signals through store-driven Ca(2+) transients to maintain synaptic homeostasis. Elife *4*, e09262. https://doi.org/10.7554/eLife.09262.
29. Brenowitz, S.D., and Regehr, W.G. (2007). Reliability and heterogeneity of calcium signaling at single presynaptic boutons of cerebellar granule cells. J. Neurosci. *27*, 7888–7898. https://doi.org/10.1523/JNEUROSCI.1064-07.2007.
30. Koester, H.J., and Sakmann, B. (2000). Calcium dynamics associated with action potentials in single nerve terminals of pyramidal cells in layer 2/3 of the young rat neocortex. J. Physiol. *529 Pt 3*, 625–646. https://doi.org/10.1111/j.1469-7793.2000.00625.x.
31. Marvin, J.S., Scholl, B., Wilson, D.E., Podgorski, K., Kazemipour, A., Müller, J.A., Schoch, S., Quiroz, F.J.U., Rebola, N., Bao, H., et al. (2018). Stability, affinity, and chromatic variants of the glutamate sensor iGluSnFR. Nat. Methods *15*, 936–939. https://doi.org/10.1038/s41592-018-0171-3.
32. D'Ascenzo, M., Fellin, T., Terunuma, M., Revilla-Sanchez, R., Meaney, D.F., Auberson, Y.P., Moss, S.J., and Haydon, P.G. (2007). mGluR5 stimulates gliotransmission in the nucleus accumbens. Proc. Natl. Acad. Sci. USA *104*, 1995–2000. https://doi.org/10.1073/pnas.0609408104.
33. Cai, Z., Schools, G.P., and Kimelberg, H.K. (2000). Metabotropic glutamate receptors in acutely isolated hippocampal astrocytes: developmental changes of mGluR5 mRNA and functional expression. Glia *29*, 70–80. https://doi.org/10.1002/(sici)1098-1136.

34. Anwyl, R. (1999). Metabotropic glutamate receptors: electrophysiological properties and role in plasticity. Brain research. Brain Res. Brain Res. Rev. *29*, 83–120. https://doi.org/10.1016/s0165-0173(98)00050-2.

35. Panatier, A., and Robitaille, R. (2016). Astrocytic mGluR5 and the tripartite synapse. Neuroscience *323*, 29–34. https://doi.org/10.1016/j.neuroscience.2015.03.063.

36. Shigemoto, R., Kinoshita, A., Wada, E., Nomura, S., Ohishi, H., Takada, M., et al. (1997). Differential presynaptic localization of metabotropic glutamate receptor subtypes in the rat hippocampus. J Neurosci *17*, 7503–7522. https://doi.org/10.1523/JNEUROSCI.17-19-07503.1997.

37. Cunha, R.A. (2001). Adenosine as a neuromodulator and as a homeostatic regulator in the nervous system: different roles, different sources and different receptors. Neurochem. Int. *38*, 107–125. https://doi.org/10.1016/s0197-0186(00)00034-6.

38. Dobrunz, L.E., and Stevens, C.F. (1997). Heterogeneity of release probability, facilitation, and depletion at central synapses. Neuron *18*, 995–1008.

39. Rudolph, S., Tsai, M.C., von Gersdorff, H., and Wadiche, J.I. (2015). The ubiquitous nature of multivesicular release. Trends Neurosci. *38*, 428–438. https://doi.org/10.1016/j.tins.2015.05.008.

40. Maschi, D., and Klyachko, V.A. (2020). Spatiotemporal dynamics of multivesicular release is determined by heterogeneity of release sites within central synapses. Elife *9*, e55210. https://doi.org/10.7554/eLife.55210.

41. Li, S., Raychaudhuri, S., Lee, S.A., Brockmann, M.M., Wang, J., Kusick, G., Prater, C., Syed, S., Falahati, H., Ramos, R., et al. (2021). Asynchronous release sites align with NMDA receptors in mouse hippocampal synapses. Nat. Commun. *12*, 677. https://doi.org/10.1038/s41467-021-21004-x.

42. Kusick, G.F., Chin, M., Raychaudhuri, S., Lippmann, K., Adula, K.P., Hujber, E.J., Vu, T., Davis, M.W., Jorgensen, E.M., and Watanabe, S. (2020). Synaptic vesicles transiently dock to refill release sites. Nat. Neurosci. *23*, 1329–1338. https://doi.org/10.1038/s41593-020-00716-1.

43. Tang, A.H., Chen, H., Li, T.P., Metzbower, S.R., MacGillavry, H.D., and Blanpied, T.A. (2016). A trans-synaptic nanocolumn aligns neurotransmitter release to receptors. Nature *536*, 210–214. https://doi.org/10.1038/nature19058.

44. Silm, K., Yang, J., Marcott, P.F., Asensio, C.S., Eriksen, J., Guthrie, D.A., Newman, A.H., Ford, C.P., and Edwards, R.H. (2019). Synaptic vesicle recycling pathway determines neurotransmitter content and release properties. Neuron *102*, 786–800.e5. https://doi.org/10.1016/j.neuron.2019.03.031.

45. Del Castillo, J., and Katz, B. (1954). Quantal components of the end-plate potential. J. Physiol. *124*, 560–573. https://doi.org/10.1113/jphysiol.1954.sp005129.

46. Katz, B. (1971). Quantal mechanism of neural transmitter release. Science *173*, 123–126. https://doi.org/10.1126/science.173.3992.123.

47. Del Castillo, J., and Katz, B. (1954). Statistical factors involved in neuromuscular facilitation and depression. J. Physiol. *124*, 574–585. https://doi.org/10.1113/jphysiol.1954.sp005130.

48. Dudel, J., and Kuffler, S.W. (1961). Mechanism of facilitation at the crayfish neuromuscular junction. J. Physiol. *155*, 530–542. https://doi.org/10.1113/jphysiol.1961.sp006645.

49. Dürst, C.D., Wiegert, J.S., Schulze, C., Helassa, N., Török, K., and Oertner, T.G. (2022). Vesicular release probability sets the strength of individual Schaffer collateral synapses. Nat. Commun. *13*, 6126. https://doi.org/10.1038/s41467-022-33565-6.

50. Oertner, T.G., Sabatini, B.L., Nimchinsky, E.A., and Svoboda, K. (2002). Facilitation at single synapses probed with optical quantal analysis. Nat. Neurosci. *5*, 657–664. https://doi.org/10.1038/nn867.

51. Vaden, J.H., Banumurthy, G., Gusarevich, E.S., Overstreet-Wadiche, L., and Wadiche, J.I. (2019). The readily-releasable pool dynamically regulates multivesicular release. Elife *8*, e47434. https://doi.org/10.7554/eLife.47434.

52. Klyachko, V.A., and Stevens, C.F. (2006). Excitatory and feed-forward inhibitory hippocampal synapses work synergistically as an adaptive filter of natural spike trains. PLoS Biol. *4*, e207. https://doi.org/10.1371/journal.pbio.0040207.

53. MacLeod, K.M. (2011). Short-term synaptic plasticity and intensity coding. Hear. Res. *279*, 13–21. https://doi.org/10.1016/j.heares.2011.03.001.

54. Gordleeva, S.Y., Tsybina, Y.A., Krivonosov, M.I., Ivanchenko, M.V., Zaikin, A.A., Kazantsev, V.B., and Gorban, A.N. (2021). Modeling working memory in a spiking neuron network accompanied by astrocytes. Front. Cell. Neurosci. *15*, 631485. https://doi.org/10.3389/fncel.2021.631485.

55. Peng, A., Rotman, Z., Deng, P.Y., and Klyachko, V.A. (2012). Differential motion dynamics of synaptic vesicles undergoing spontaneous and activity-evoked endocytosis. Neuron *73*, 1108–1115. https://doi.org/10.1016/j.neuron.2012.01.023.

56. Yang, Y., Ge, W., Chen, Y., Zhang, Z., Shen, W., Wu, C., Poo, M., and Duan, S. (2003). Contribution of astrocytes to hippocampal long-term potentiation through release of D-serine. Proc. Natl. Acad. Sci. USA *100*, 15194–15199. https://doi.org/10.1073/pnas.2431073100.

57. Aguet, F., Antonescu, C.N., Mettlen, M., Schmid, S.L., and Danuser, G. (2013). Advances in analysis of low signal-to-noise images link dynamin and AP2 to the functions of an endocytic checkpoint. Dev. Cell *26*, 279–291. https://doi.org/10.1016/j.devcel.2013.06.019.

58. Jaqaman, K., Loerke, D., Mettlen, M., Kuwata, H., Grinstein, S., Schmid, S.L., and Danuser, G. (2008). Robust single-particle tracking in live-cell time-lapse sequences. Nat. Methods *5*, 695–702. https://doi.org/10.1038/nmeth.1237.

59. Schmidhuber, J. (2015). Deep learning in neural networks: an overview. Neural Netw. *61*, 85–117. https://doi.org/10.1016/j.neunet.2014.09.003.

STAR★METHODS

KEY RESOURCES TABLE

REAGENT or RESOURCE	SOURCE	IDENTIFIER
Bacterial and virus strains		
pFU-vGluT1-pHGFP-W	Viral Vectors Core at Washington University	N/A
pFU-vMAT2-pHGFP-W	Viral Vectors Core at Washington University	N/A
pAAV.hSynapsin.SF-iGluSnFR.A184S	Addgene	Cat.No. 106174-AAV1
pAAV.GFAP.SF-iGluSnFR.A184S	Addgene	Cat.No. 106192-AAV1
Biological samples		
Hippocampus of Long-Evans rat pups	Charles River	Cat.No. 006
Chemicals, peptides, and recombinant proteins		
APV	Sigma-Aldrich	Cat.No. 79055-68-8
CNQX disodium salt hydrate	Sigma-Aldrich	Cat.No. 115066-14-3
HEPES	Sigma-Aldrich	Cat.No. 7365-45-9
D-(+)-Glucose	Sigma-Aldrich	Cat.No. 50-99-7
Calcium chloride dihydrate	Sigma-Aldrich	Cat.No. 10035-04-8
Magnesium chloride hexahydrate	Sigma-Aldrich	Cat.No. 7791-18-6
Minimum Essential Media (MEM) -No phenol Red	Gibco™	Cat.No. 51200038
Characterized Fetal Bovine Serum	Gibco™	Cat.No. 10437028
Penicillin-Streptomycin (5, 000 U/mL)	Gibco™	Cat.No. 15070063
N-2 Supplement (100x)	Gibco™	Cat.No. 17502048
Donor Equine Serum	HyClone	Cat.No. SH30074.03
Sodium Pyruvate (100 mM)	CORNING	Cat.No. 25-000-CI
Neurobasal-A Medium	Gibco™	Cat.No. 12349015
B-27 supplement (50x), serum free	Gibco™	Cat.No. 17504044
GlutaMAX Supplement	Gibco™	Cat.No. 35050061
Earle's Balanced Salts	Sigma-Aldrich	Cat.No. E3024
Collagen Type I, Rat Tail	CORNING	Cat.No. 354236
Cover Glasses	Thermo Fisher Scientific	Cat.No. 12-545-80
Papain	Worthington Biochemical	Cat.No. LS003126
PDL(poly-D-lysine)	BD Biosciences	Cat.No. 40210
Trypsin-EDTA (0.05%), phenol red	Gibco™	Cat.No. 25300054
MPEP hydrochloride	Sigma-Aldrich	Cat.No. 219911-35-0
MTEP hydrochloride	Sigma-Aldrich	Cat.No. M4699
CPPG	Thermo Fisher Scientific	Cat.No. 09.725
DPCPX	Sigma-Aldrich	Cat.No. 102146-07-6
SCH 58261	Sigma-Aldrich	Cat.No. 160098-96-4
DL-threo-β-Hydroxyaspartic acid	Sigma-Aldrich	Cat.No. 4294-45-5
CultureOne™ Supplement (100x)	Thermo Fisher Scientific	Cat.No. A3320201
CGS-21680	Sigma-Aldrich	Cat.No. 124182-57-6
AOPCP	Sigma-Aldrich	Cat.No. 104835-70-3
ADX-47273	Sigma-Aldrich	Cat.No. 851881-60-2
UCPH-102	Sigma-Aldrich	Cat.No. 1229591-56-3
Recombinant DNA		
VGlut1-pHluorin	Voglmaier et al.[20]	N/A
vMAT2-pHluorin	Silm et al.[44]	N/A

(*Continued on next page*)

Continued

REAGENT or RESOURCE	SOURCE	IDENTIFIER
Software and algorithms		
MATLAB	MathWorks	RRID: SCR_001622
u-track 2.0	https://www.utsouthwestern.edu/labs/danuser/software/#utrack_anc	Gaudenz Danuser Lab
ImageJ	https://imagej.nih.gov/ij/	RRID: SCR_003070
Fiji	http://fiji.sc	RRID: SCR_002285

RESOURCE AVAILABILITY

Lead contact

Further information and requests for resources and reagents should be directed to and will be fulfilled by the lead contact, Dr. Vitaly A. Klyachko (klyachko@wustl.edu).

Materials availability

This study did not generate new or unique reagents or other materials.

Data and code availability

- This paper does not report standardized data types. All data reported in this paper will be shared by the lead contact upon request.
- This paper does not report stand alone custom code. MATLAB was used to appropriately organize, process, and analyze data and corresponding routines are available from the lead contact upon request.
- Any additional information required to reanalyze the data reported in this paper is available from the lead contact upon request.

EXPERIMENTAL MODEL AND SUBJECT DETAILS

Primary neuronal cultures were produced from the hippocampus of Long-Evans rat pups (Charles River, strain code #006) of both sexes.[23,55] Hippocampi were dissected from E16-17 pups, dissociated by papain digestion, and plated on glass coverslips. Neurons were cultured in Neurobasal media supplemented with B-27 supplement. Three types of hippocampal neuronal cultures were used in the present study. (i) The neuron/astrocyte co-culture, in which neurons were grown on top of a confluent astrocyte monolayer prepared as described.[23,55] (ii) Neuron-only culture as described,[56] with minor modifications. These cultures were treated with CultureOne Supplement to kill proliferating cells. (iii) ACM cultures, prepared and cultured in the same manner as neuron-only cultures except that, after one week, one coverslip prepared for neuron-only culture and three coverslips with a confluent layer of astrocyte cultures were cultured side-by-side in a single 35-mm dish as described.[56] All animal procedures were in compliance with the US National Institutes of Health Guide for the Care and Use of Laboratory Animals, and conformed to the guidelines approved by the Washington University Animal Studies Committee, protocol #20–0173.

METHOD DETAILS

Lentiviral infection

VGlut1-pHluorin and vMAT2-pHluorin were generously provided by Drs. Robert Edwards and Susan Voglmaier (UCSF).[20,44] SF-iGluSnFR(A184) and GFAP.SF-iGluSnFR(A184S) were kindly made available by Dr. Loren Looger (Addgene viral prep #106174-AAV1 and #106192-AAV1).[31] Lentiviral vectors were generated by the Viral Vectors Core at Washington University. Hippocampal neuronal cultures were infected at DIV3 as described.[22,23,40]

Near-TIRF microscopy

All near-total internal reflection fluorescence (near-TIRF) experiments were conducted at 37°C within a whole-microscope incubator chamber (TOKAI HIT). Individual release events were evoked by 1Hz field stimulation for 200s, unless noted otherwise. Fluorophores were excited with a 488 laser (Cell CMR-LAS-488, Olympus), and monitored using an inverted TIRF-equipped microscope (IX83, Olympus) under a 150x/1.45NA objective (UApo N). The Z-drift compensation system (IX3-ZDC) was used to ensure constant position of the focal plane during imaging. Near-TIRF with a penetration depth of <1 μm was achieved by adjusting the incident angle to 63.7°, which is near the critical angle of 63.6°. Images were acquired every 50 ms (with an exposure time of 49.38 ms) using a cooled EMCCD camera (iXon life 888, ANDOR). Field simulation was performed by using a pair of platinum electrodes and controlled by the software via Master-9 stimulus generator (A.M.P.I.). Samples were perfused with bath solution (125 mM NaCl, 2.5 mM KCl, 2mM $CaCl_2$, 1mM $MgCl_2$, 10 mM HEPES, 15mM Glucose, 50 μM APV, 10 μM CNQX adjusted to pH 7.4).

Experimental design

Experiments with two conditions were performed in parallel on the same day (i.e., control vs pharmacological compound) using the same day cultures. All experiments were designed and performed with an internal control by comparing changes in Pr within the same synapse, i.e., by comparing Pr after release events relative to Pr after failures. These internally controlled measurements are thus largely independent of day-to-day variations in culture conditions. Moreover, the basal Pr also shows very little variation from culture-to-culture in our measurements with no statistically significant differences among different cultures/days ($p > 0.49$ for all, ANOVA). Similarly, the distribution of the number of consecutive release events detected in each bouton in control conditions, which represents a measure of release-dependent facilitation, shows no significant differences among different cultures/days ($p > 0.53$ for all, K-S test). The control measurements were therefore pooled.

Pharmacology

THA and EGTA-AM were diluted in dimethyl sulfoxide (DMSO) and stored at −20°C. UCPH-102, MPEP, and MTEP were diluted in DMSO and stored at 4°C. CPPG, DPCPX, and SCH 58261 were diluted in DMSO and stored at room temperature. Samples were pre-incubated in imaging solution with 100 μM of THA, 10 μM of UCPH-102, 250 μM of MPEP, 250 μM of MTEP, 100 nM CPPG, 25 μM EGTA-AM, 100 μM AOPCP, 1 mM DPCPX, 100 nM SCH 58261, 100 nM CGS-21680, and 1 μM ADX-47273, for 30 min prior to the beginning of the recordings. The effective final DMSO concentration was <0.5%.

QUANTIFICATION AND STATISTICAL ANALYSES

Event detection and localization using mixture-model fitting

VGlut1-pHluorin- and vMAT2-pHluorin–based release event detection and localization at subpixel resolution were performed as described[22,23,40] using MATLAB and the uTrack software package, which was kindly made available by Dr Gaudenz Danuser's lab.[57,58] Localization precision was determined directly from least-squares Gaussian fits of individual events as described.[23,40] Detection of synaptic glutamate release in neurons using SF-iGluSnFR(A184) was performed using the same approach as described above.

Event detection using deep learning algorithm

To confirm results obtained with the mixture-model fitting approach, event detection was also performed independently using a deep learning algorithm, available in MATLAB.[59] Training of the deep learning algorithm was performed using a feedforward neural network with 1,000 maximum epochs. This algorithm updates weight and bias values according to the conjugate gradient back propagation with Powell-Beale restarts. The performance function, called loss function, used mean squared error to train the algorithm. The hidden layer size was 100, and the output layer size was two, event and failure. Well-defined images and intensity traces of 10,000 events and 10,000 failures each were used to train the neural network. The uTrack software package was used to define events and failures. Three kinds of inputs were used for training (1) event or failure, (2) corresponding intensity of the fluorescence signal for 1s (3) corresponding image stacks for 1sec. The inputs were divided into training, validation, and test input, and the ratio was 0.7: 0.15: 0.15 randomly. Upon training the algorithm achieved 96.0% of correct predictions (Figure S1).

Event detection using ROI thresholding

This approach followed the published event detection algorithm[28] with minor modifications. To determine synapse locations, the stack of all 4,000 frames in each movie was summed to create a combined image, and localizations of individual synapses were defined as local peaks in the combined image using ImageJ. Whole-synapse VGlut1-pHluorin intensity was measured over a 0.95 μm diameter circle (11 pixels) region of interest (ROI) centered on each bouton. A threshold on the ROI intensity was set at 0.15 ΔF/F. Only ROIs with a peak amplitude greater than 2 standard deviations for the previous 1 s were accepted. Finally, instantaneous slopes of ROI fluorescence changes were calculated frame-by-frame, and detection threshold was set at 0.1 Δa.u./frame. An event was accepted only when all three criteria were met: the ROI intensity, slope, and 2 standard deviations criteria.[28]

Virtual model synapse

The release events were generated by a virtual synapse model in MATLAB with the same average Pr, and the same number of events as each experimental synapse, but distributed randomly in time. 1,732 virtual synapses were analyzed using an identical appoach in Utrack software as experimental ones.

Identification and analysis of MVR events

We used a well-defined biGaussian fitting approach of the release event amplitude distribution to define a relative proportion of UVR and MVR events (Figures 3C and 3D).[40] Amplitudes of peak fluorescence signal were converted to biGaussian function as follows:

$$Y = a_1 * \exp(-((x - b_1)/c_1)^2 + a_2 * \exp(-((x - 2 * b_1)/c_1)^2$$

where a_1 and a_2 are amplitude of UVR and MVR, b_1 and $2*b_1$ are the centers of UVR and MVR, and c_1 is related to the peak width. The threshold for identification of an event as MVR was set at two standard deviations above the mean event amplitude determined individually for each bouton (Figure 3B).

Analysis of event spatial organization

The AZ size was approximated based on the convex hull encompassing all vesicle fusion events in a given bouton. This measurement is in a close agreement with the ultrastructural measurements of AZ dimensions.[23] AZ center was defined as the mean position of all fusion events in a given bouton.

Release sites were defined using hierarchical clustering algorithm with a cluster diameter of 50 nm using built-in functions in MATLAB as described.[22,23,40] We have previously shown that the observed clusters do not arise from random distribution of release events, but rather represent a set of defined and repeatedly reused release sites within the AZs.

In the analyses comparing spatial properties of burst events vs isolated events, since the first event in each burst was not immediately preceded by another successful release event, it cannot be assumed to be evoked as a result of astrocyte-dependent facilitation. Thus these first events in each burst were excluded from the spatial analyses of burst events.

Analysis of glutamate transients in astrocytes

For detection of glutamate transients in astrocytes using GFAP.SF-iGluSnFR(A184), each movie stack was merged in ImageJ to create a single image. ROIs were defined based on this composite image as areas encompassing at least 80% of maximum fluorescence intensity. For each 1Hz, 120 s recording, ROI intensities were determined for one frame before and one frame after each stimulation, and the two sets were compared with a paired-sample *t* test to determine if a given cell had evoked glutamate transients. For presentation (Figure S2F and S2I), each 1s trace was divided by an average intensity of three frames immediately preceding the stimulation.

Data inclusion and exclusion criteria

A minimum of 10 detected release events per bouton was required for all analyses. A minimum of 15 detected release events per bouton was required for analysis of spatial properties of events in Figures 4E–4G.

Statistical analysis

Statistical analyses were performed in MATLAB. Statistical significance was determined using a two-sample two-tailed t test, Tukey-Kramer ANOVA, and Kolmogorov-Smirnov(K-S) tests where appropriate. Statistical tests used to measure significance, the corresponding significance level (p-value), and the values of n are provided for each panel in Table S1. Data are reported as mean ± SEM, and $p < 0.05$ was considered statistically significant.